Progress towards a large eddy simulation of premixed turbulent combustion in stagnating turbulence

By D. S. Louch

1. Motivation and objectives

Large eddy simulations (LES) of premixed turbulent combustion (PTC) is a relatively recent and unexplored field with the potential to improve predictions for flows where classical Reynolds-averaged Navier Stokes approaches (RANS) have lacked precision. Examples of applications particularly well suited for LES of PTC include the unsteady nature of the flow in an IC engine or the large unsteady vortical structures in modern gas turbines where LES of PTC has the potential to predict occurrences of undesirable acoustic instabilities and test active and passive control techniques (Veynante and Poinsot, 1997; Angelberger *et al.*, 1998).

Many premixed turbulent combustion configurations lie within the flamelet regime where the structure of the premixed turbulent flame brush resembles a strongly wrinkled and stretched laminar flame dynamically changing topology in the turbulent flow. Resolution of the flame in this regime requires resolving the thin dynamic flame front which is often between $0.1mm$ and $1.0mm$ thick and thus often less than the grid spacing desired in large eddy simulations of practical combustion chambers. To overcome this difficulty a number of techniques have been proposed although few have been used in realistic configurations.

The objective of this work is to contribute to the development of LES of PTC by investigating the simulation of a premixed turbulent flame brush in stagnating turbulence (Bray *el al.*, 1994). A general schematic of this configuration is shown in Fig. 1. Grid generated isotropic turbulence is created at a jet nozzle exit and impinges on a plate a distance from the nozzle exit on the order of one nozzle diameter. Often a co-flow of inert gas surrounds the reactive core flow, preventing structures that would develop in the shear layer at the edge of the reactive core flow from disrupting the reactive isotropic turbulence. A premixed turbulent flame brush is then stabilized in the vicinity in front of the plate. This configuration is closely related to the opposing streams configuration (Bray *et al.*, 1991; Kostiuk *el al.*, 1999) where a stagnation flow is formed by opposing turbulent jet streams. The stagnation flow configuration is one of three commonly used configurations (the classical Bunsen flame and the V-flame configurations being the other two) in experimental laboratory studies of premixed turbulent combustion (Cheng and Shepherd, 1991). Theoretical work (Bray *et al.*, 1998; Bray *et al.*, 1999) and RANS simulations (Lindstedt and Vaos, 1998; Lindstedt and Vaos, 1999) have been reported in the literature and numerous direct numerical simulations (DNS) of PTC (Haworth and Poinsot, 1992; Rutland and Cant, 1994; Trouvé and Poinsot, 1994; Zhang and Rutland, 1995; Poinsot *et al.*, 1996; Echekki and Chen, 1996; Veynante

and Poinsot, 1997b; Veynante *et al.*, 1997; Boughanem and Trouvé, 1998; Chen and Im, 1998; Chen and Echekki and Kollmann; 1999; Helie and Trouvé, 1998) consider a freely propagating planar turbulent flame brush resembling the planar turbulent flame brush formed in stagnating turbulence.

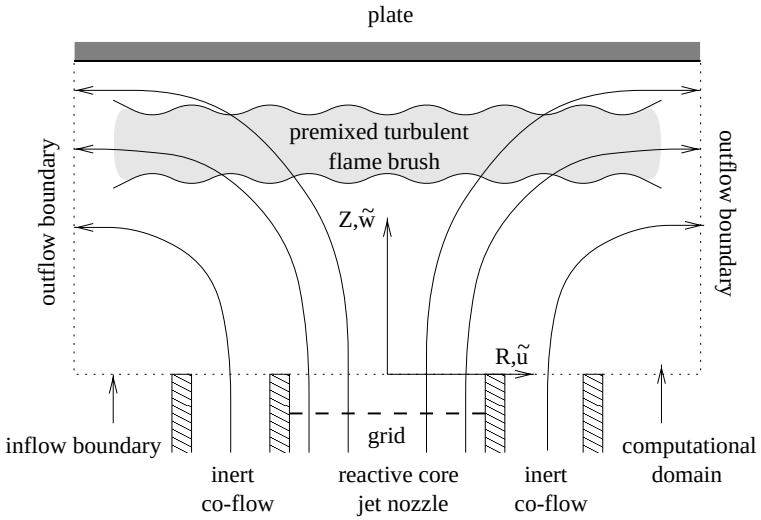

FIGURE 1. Schematic diagram of the computational domain and an experimental premixed turbulent flame brush in stagnating turbulence.

A number of the current techniques proposed to deal with the resolution problem in any large eddy simulation of premixed turbulent combustion in the flamelet regime are commented on below.

1.1 The field equation approach

The field equation (or "G-equation" as it is commonly referred to) approach (Peters, 1992; Smith and Menon, 1996; Im and Lund, 1997) treats the flame as an infinitely thin sheet separating burnt and unburnt gas propagating normal to itself at a convective velocity S_L, determined *a priori*, which is usually a function of the turbulence intensity. Appropriate jump conditions across the flame sheet are required, and special consideration must be given to either deal with or remove the formation of cusps which naturally arise in solutions of the basic field equation

$$\frac{\partial G}{\partial t} + u_i \frac{\partial G}{\partial x_i} = S_L \left| \nabla G \right|,$$

where $G = G(x,t)$ and $G(x,t) = G_o$ denotes the flame sheet.

1.2 The random vortex approach

The random vortex approach is a grid-free Lagrangian approach (Givi, 1994) where chemistry may be handled by following flame elements and is suitable for the LES of PTC (Rhee *et al.*, 1995).

1.3 The flame surface density approach

The flame surface density (Pope, 1988) approach is based upon filtering the basic equations with a filter width sufficiently larger than the grid spacing such that the thin turbulent dynamic premixed flame is smeared out sufficiently to be resolved on a LES grid. A model is then required for the flame surface density and can be provided through either an algebraic expression or solving a transport equation for the flame surface density (Trouvé and Poinsot, 1994; Prasad and Gore, 1999). This approach is very attractive in that it is consistent with the LES philosophy. Topological features of the flame with sufficiently large length scales are resolved and subgrid scale topological features are absorbed in subgrid scale models. The approach avoids artificial flame thickening as in the thickened flame models discussed next: however, the level of modeling complexity can be significantly increased if the filtered transport equation for the flame surface density (Boger *et al.*, 1998) is used.

1.4 The thickened flame approach

The current thickened flame model (Butler and O'Rourke, 1977; Veynante and Poinsot,1997; Angelberger, 1998; Colin and Ducros, 1999) involves two steps:

Step 1: Artificially thicken the flame sufficiently for resolution on a LES grid while preserving the laminar burning velocity of the flame.

Step 2: Modify the laminar burning velocity of the thickened flame to take into account subgrid scale wrinkles by multiplying the preexponential factor by an efficiency factor such that the flame burns at subgrid scale turbulent burning velocity.

The first step is accomplished by decreasing the Prandtl number sufficiently to increase the effective diffusivity of the gas producing a laminar flame sufficiently thick for resolution on a LES grid and decreasing the preexponential factor to preserve the laminar burning velocity of the flame. An Arrhenius reaction rate expression is used with the filtered quantities. This technique has been used by Angelberger *et al.* (1998) and Veynante and Poinsot (1997) in configurations where there is no mixing between the reactive gas and inerts before the reactants are burned at the flame front. However, in configurations where mixing takes place with inerts prior to combustion, as in the stagnating turbulence configuration considered here, this technique increases the diffusion of reactants from the core jet to the surrounding gas to unacceptable levels. A new thickened flame approach has been developed to overcome this problem and will be discussed below. Models have been proposed for the second step to account for the increased burning velocity of the flame due to subgrid scale wrinkling by Angelberger *et al.* (1998) and Colin and Ducros *et al.* (1999).

1.5 LES combustion equations

The zero Mach number set of combustion equations

$$\frac{\partial \rho}{\partial t} + \frac{\partial \rho u_j}{\partial x_j} = 0 \ , \tag{1}$$

$$\frac{\partial \rho u_i}{\partial t} + \frac{\partial \rho u_i u_j}{\partial x_j} = -\frac{\partial p}{\partial x_i} + \frac{1}{Re}\frac{\partial 2\mu d_{ij}}{\partial x_j} + \frac{1}{Fr}\rho F_i \ , \tag{2}$$

$$\frac{\partial \rho T}{\partial t} + \frac{\partial \rho u_j T}{\partial x_j} = \frac{1}{RePr}\frac{\partial}{\partial x_j}\left(\mu \frac{\partial T}{\partial x_j}\right) + w_P + Q \ , \tag{3}$$

$$\frac{\partial \rho Y_R}{\partial t} + \frac{\partial \rho u_j Y_R}{\partial x_j} = \frac{1}{RePrLe}\frac{\partial}{\partial x_j}\left(\mu \frac{\partial Y_R}{\partial x_j}\right) - w_P \ , \tag{4}$$

$$\rho\left[\left(\frac{\alpha}{1-\alpha}\right)T + 1\right] = 1 \ , \tag{5}$$

$$w_P = B\rho Y_R exp\left(\frac{-\beta(1-T)}{1-\alpha(1-T)}\right) \ , \tag{6}$$

$$d_{ij} = (S_{ij} - \frac{1}{3}S_{kk}\delta_{ij}) \ , \tag{7}$$

$$S_{ij} = \frac{1}{2}\left(\frac{\partial u_i}{\partial x_j} + \frac{\partial u_j}{\partial x_i}\right) \ , \tag{8}$$

written in Cartesian nondimensional form describe an ideal gas mixture of two components reacting under the single-step mechanism $R \rightarrow P$ with the rate of formation of product, w_P, given by an Arrhenius reaction rate expression. In these equations ρ is the density, u_j is the velocity in the x_j direction, p is the pressure, μ is the viscosity, F_i is a body force in the x_i direction, T is the temperature, Q is a heat source, Y_R is the mass fraction of the reactant R, α is a temperature factor equal to $(T_b^* - T_u^*)/T_b^*$ where subscripts b and u refer to the burnt and unburnt gas respectively (quantities denoted with the $*$ superscript are dimensional), β is an activation energy, B is the preexponential factor, $2\mu d_{ij}$ is the deviatoric stress tensor, S_{ij} is the strain rate tensor, and δ_{ij} is the Kronecker delta function. The nondimensional numbers

$$Re = \frac{\rho_{ref}^* l_{ref}^* u_{ref}^*}{\mu_{ref}^*}; \quad Pr = \frac{\mu_{ref}^* C_p^*}{\lambda_{ref}^*}; \quad Sc = \frac{\mu_{ref}^*}{\rho_{ref}^* D_{RP,ref}^*}; \quad Le = \frac{Sc}{Pr}; \quad Fr = \frac{u_{ref}^{*^2}}{l_{ref}^* g^*}$$

are respectively the Reynolds, Prandtl, Schmidt, Lewis, and Froude numbers, where l_{ref}^* is a reference length scale, C_p^* is the specific heat capacity, λ_{ref}^* is a reference thermal conductivity, $D_{RP,ref}^*$ is a reference molecular diffusivity, and g^* is the acceleration due to gravity.

For variable density flows the basic LES equations are simplified when Favre filtering a quantity $f(x,t)$, given by the operation

$$\bar{\rho}\tilde{f} = \overline{\rho f} = \int_{-\infty}^{+\infty} \rho f(x,t) G(x-x')dx',$$

is used in place of the basic filtering operation

$$\bar{f}(x,t) = \int_{-\infty}^{+\infty} f(x',t) G(x-x')dx'.$$

Favre filtering the above equations leads to the set

$$\frac{\partial \bar{\rho}}{\partial t} + \frac{\partial \bar{\rho}\tilde{u}_j}{\partial x_j} = 0 \ , \tag{9}$$

$$\frac{\partial \bar{\rho}\tilde{u}_i}{\partial t} + \frac{\partial \bar{\rho}\tilde{u}_i\tilde{u}_j}{\partial x_j} = -\frac{\partial \bar{p}}{\partial x_i} + \frac{1}{Re}\frac{\partial 2\tilde{\mu}\tilde{d}_{ij}}{\partial x_j} - \frac{\partial \tau_{ij}}{\partial x_j} + \frac{1}{Fr}\bar{\rho}\tilde{F}_i \ , \tag{10}$$

$$\frac{\partial \bar{\rho}\tilde{T}}{\partial t} + \frac{\partial \bar{\rho}\tilde{u}_j\tilde{T}}{\partial x_j} = \frac{1}{RePr}\frac{\partial}{\partial x_j}\left(\tilde{\mu}\frac{\partial \tilde{T}}{\partial x_j}\right) - \frac{\partial \bar{\rho}(\widetilde{u_jT} - \tilde{u}_j\tilde{T})}{\partial x_j} + \bar{w}_P + \bar{Q} \ , \tag{11}$$

$$\frac{\partial \bar{\rho}\tilde{Y}_R}{\partial t} + \frac{\partial \bar{\rho}\tilde{u}_j\tilde{Y}_R}{\partial x_j} = \frac{1}{RePrLe}\frac{\partial}{\partial x_j}\left(\tilde{\mu}\frac{\partial \tilde{Y}_R}{\partial x_j}\right) - \frac{\partial \bar{\rho}(\widetilde{u_jY_R} - \tilde{u}_j\tilde{Y}_R)}{\partial x_j} - \bar{w}_P \ , \tag{12}$$

$$\bar{\rho}\left[\left(\frac{\alpha}{1-\alpha}\right)\tilde{T} + 1\right] = 1 \ , \tag{13}$$

$$\bar{w}_P = \overline{B\rho Y_R exp\left(\frac{-\beta(1-T)}{1-\alpha(1-T)}\right)} \ , \tag{14}$$

of simple chemistry zero Mach number LES combustion equations, where $\tau_{ij} = \bar{\rho}(\widetilde{u_iu_j} - \tilde{u}_i\tilde{u}_j)$ and the molecular diffusive terms in the momentum, energy, and species equations have been approximated following Erlebacher *et al.* (1990). In the current simulations the viscosity $\tilde{\mu}$ is kept constant; however, a temperature dependent viscosity of the form $\tilde{\mu} = (\tau\tilde{T} + 1)^b$, where $\tau = (T_b^* - T_u^*)/T_u^*$ and b is a model constant usually taken to be 0.76 (Haworth and Poinsot, 1992), will be used in future simulations.

The subgrid scale stresses are modeled with the Smagorinsky model

$$\tau_{ij} - \frac{1}{3}\tau_{kk}\delta_{ij} = -2C\bar{\Delta}^2\bar{\rho}|\tilde{S}_{ij}|\tilde{d}_{ij} \ , \tag{15}$$

where C is either constant (classical Smagorinsky model) or can be determined by the dynamic procedure (Germano *et al.*, 1991; Germano, 1992; Akselvoll and Moin, 1995). The subgrid scale turbulent fluxes are modeled with the eddy diffusivity models

$$\bar{\rho}(\widetilde{u_jT} - \tilde{u}_j\tilde{T}) = -\frac{C\bar{\Delta}^2\bar{\rho}|\tilde{S}_{ij}|}{Pr_t}\frac{\partial \tilde{T}}{\partial x_j} \tag{16}$$

and

$$\bar{\rho}(\widetilde{u_jY_R} - \tilde{u}_j\tilde{Y}_R) = -\frac{C\bar{\Delta}^2\bar{\rho}|\tilde{S}_{ij}|}{Sc_t}\frac{\partial \tilde{Y}_R}{\partial x_j} \ , \tag{17}$$

where Pr_t and Sc_t are the turbulent Prandtl and Schmidt numbers respectively taken to be unity. The author acknowledges that eddy diffusivity models for the subgrid scale turbulent scalar fluxes is purely heuristic and further study is required to reveal the nature of these fluxes, particularly given that in Reynolds averaged studies the turbulent scalar flux can exhibit either gradient or countergradient transport behavior depending upon turbulence intensities and the presence of mean pressure gradients (Veynante *et al.*, 1997; Veynante and Poinsot, 1997b; Louch and Bray, 1998; Louch, 1998; Louch *et al.*, 1999).

2. Accomplishments

Closure of the above LES combustion equations require a model for the reaction rate $\bar{w}_P$. As discussed above, in the current configuration an inert co-flow surrounds the reactive isotropic turbulent core flow and current thickened flame models result in excessive diffusion of the reactive core flow to the inert co-flow.

2.1 The adaptive thickened flame approach

To overcome the global strongly diffusive nature of previous thickened flame models, an adaptive thickened flame approach has been developed. Let $\delta_{t,SGS}$ denote the flame thickness of the thickened simulated flame, $S_{t,SGS}$ denote the burning velocity of the thickened flame, and $\bar{\Delta}$ denote the grid spacing. The desired properties for an adaptive thickened flame model are:

Property 1. A thickened flame with a laminar flame thickness that dynamically adjusts to the grid spacing such that $\delta_{t,SGS} = N_f \bar{\Delta}$, where N_f is the number of grid points desired to resolve the flame and is independent of $\bar{\Delta}$. This property preserves the resolution of the flame in nonuniform grids.

Property 2. Preserve the invariance of the laminar burning velocity of the flame with respect to $\bar{\Delta}$.

To accomplish the first property, the thermal and molecular diffusivity is augmented by an expression which depends on the magnitude of the temperature gradient and the grid spacing. Realization of the second property is accomplished by dividing the reaction rate by the grid spacing raised to an appropriate power. The objective here in this flame thickening approach is not the modeling of any subgrid scale diffusivity using this technique, but to simply construct a premixed flame with the above properties. Future investigations will consider other approaches which avoid artifical flame thickening by addressing the modeling of the reaction rate, w_P, using non-Arrhenius type models.

Consider the modified energy and species equations

$$\frac{\partial \rho T}{\partial t} + \frac{\partial \rho u_j T}{\partial x_j} = \frac{\partial}{\partial x_j}\left\{\left(\frac{1}{RePr} + C_f \bar{\Delta}^{\alpha_1} \rho B \left|\frac{\partial T}{\partial x_j}\right|\right)\frac{\partial T}{\partial x_j}\right\} + \frac{1}{\bar{\Delta}^{\alpha_2}} w_P \ , \tag{18}$$

$$\frac{\partial \rho Y_R}{\partial t} + \frac{\partial \rho u_j Y_R}{\partial x_j} = \frac{\partial}{\partial x_j}\left\{\left(\frac{1}{RePrLe} + C_f \bar{\Delta}^{\alpha_1} \rho B \left|\frac{\partial T}{\partial x_j}\right|\right)\frac{\partial Y_R}{\partial x_j}\right\} - \frac{1}{\bar{\Delta}^{\alpha_2}} w_P \ , \tag{19}$$

where

$$w_P = B \rho Y_R exp\left(\frac{-\beta(1-T)}{1-\alpha(1-T)}\right) \ , \tag{20}$$

$$\left|\frac{\partial T}{\partial x_j}\right| = \sqrt{\frac{\partial T}{\partial x_j}\frac{\partial T}{\partial x_j}} \ , \tag{21}$$

C_f is a model constant determining N_f, and α_1 and α_2 are constants to be determined such that the first and second properties are satisfied.

2.2 The numerical method

A code has been developed to numerically solve the modeled set of LES zero Mach number combustion equations, Eqs. (9)-(17), in cylindrical coordinations. A second order finite volume discretization is used on a staggered cylindrical grid with velocities advanced at cell surfaces and scalars at cell centers. A fully explicit predictor-corrector scheme is used to advance the equations with a direct solver for the Poisson equation which arises from the zero Mach number formulation. During the predictor and corrector steps, a fractional-step scheme is used for the scalar transport equations.

2.3 One-dimensional results

Shown in Fig. 2 is a comparison between the structure of a laminar one-dimensional planar flame from DNS, i.e. $C_f, \alpha_2 = 0.0$, and the structure of a laminar one-dimensional adaptive thickened flame with $\alpha_1 = 2.0$ and $\alpha_2 = 0.9$. Due to the dependency of the diffusivity on the temperature gradient, the species and temperature profiles show a sharper decline and rise respectively at the cold side of the adaptive thickened flame.

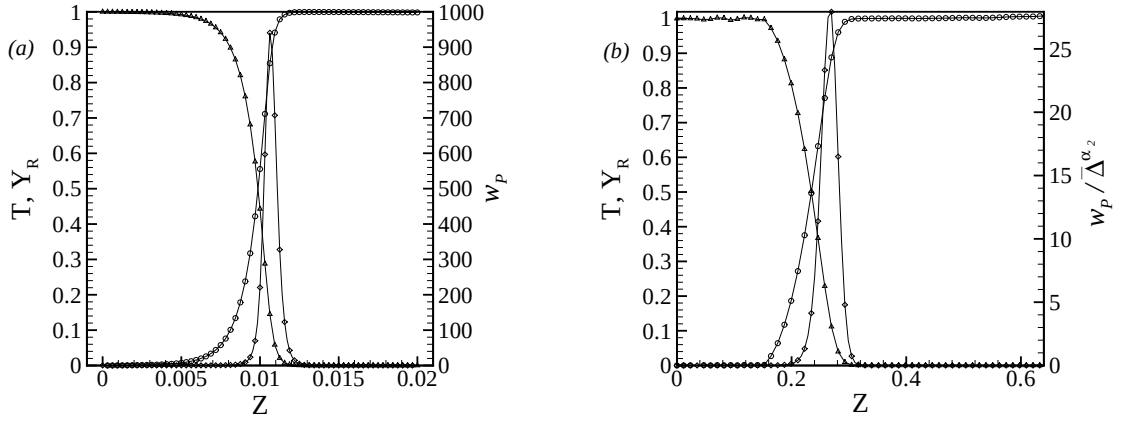

FIGURE 2. One-dimensional laminar flame profiles of temperature, T ($\circ$), species mass fraction, Y_R ($\triangle$), and reaction rate, w_P ($\diamond$), from: (a) DNS with $C_f = 0.0$, $\alpha_2 = 0.0$, $N_z = 64$, $L_z = 0.02$, $Re = 1400.0$, $Pr = 0.7$, $Le = 1.0$, $\alpha = 0.4$, $\beta = 7.0$, $B = 30000$: (b) adaptive thickened flame approach with $C_f = 2.54$, $\alpha_1 = 2.0$, $\alpha_2 = 0.9$, $N_z = 64$, $L_z = 0.75$, $Re = 1400.0$, $Pr = 0.7$, $Le = 1.0$, $\alpha = 0.4$, $\beta = 7.0$, $B = 16.5$ (N_z and L_z are the number of grid points used and the size of the computational domain respectively).

Shown in Fig. 3 is a plot of the behavior of $N_f = \delta_{t,SGS}/\bar{\Delta}$ and $S_{t,SGS}$ as a function of the grid spacing $\bar{\Delta}$ for a one-dimensional adaptive thickened laminar flame. As can be seen from this figure both the first and second properties are closely satisfied with these values of α_1 and α_2.

Shown in Fig. 4 is the behavior of N_f and $S_{t,SGS}$ as a function of Reynolds number. As the Reynolds number decreases, the magnitude of the molecular diffusive term in the diffusivity expression approaches the same order as the thickening

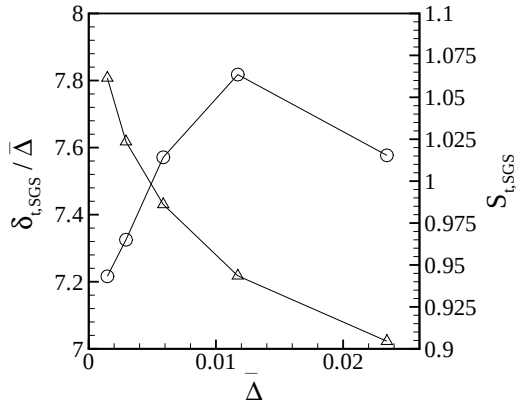

FIGURE 3. Behavior of N_f ($\triangle$) and $S_{t,SGS}$ ($\bigcirc$) as a function of $\bar{\Delta}$ for a one-dimensional adaptive thickened flame with $L_z = 0.75$, $Re = 20000$, $Pr = 0.7$, $Le = 1.0$, $C_f = 2.54$, $\alpha_1 = 2.0$, $\alpha_2 = 0.9$, $\alpha = 0.4$, $\beta = 7.0$, $B = 16.5$: Values of $\bar{\Delta}$ correspond to simulations with $N_z = 32, 64, 128, 256$, and 512.

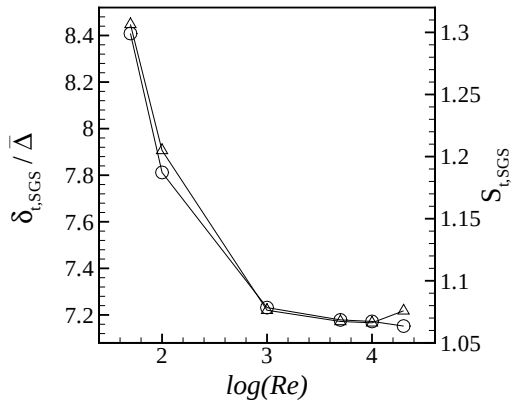

FIGURE 4. Behavior of $N_f = \delta_{t,SGS}/\bar{\Delta}$ ($\triangle$) and $S_{t,SGS}$ ($\bigcirc$) as a function of $log(Re)$ for a one-dimensional adaptive thickened flame with $N_z = 64$, $L_z = 0.75$, $Pr = 0.7$, $Le = 1.0$, $C_f = 2.54$, $\alpha_1 = 2.0$, $\alpha_2 = 0.9$, $\alpha = 0.4$, $\beta = 7.0$, $B = 16.5$: Values of $log(Re)$ correspond to $Re = 50, 100, 1000, 5000, 10000$, and 20000.

diffusive term and N_f and $S_{t,SGS}$ become Reynolds number dependent.

Shown in Fig. 5 is the behavior of N_f and $S_{t,SGS}$ as a function of the preexponential factor B. The resolution of the adaptive thickened flame is reasonably constant while $S_{t,SGS}$ shows a strongly linear dependence on B. With the adaptive thickened flame used in place of the current thickened flame approach, the preexponential factor can be modified in a manner analogous to that used by Veynante and Poinsot (1997) and Angelberger *et al.* (1998) in their thickened flame approach, as outlined above in Steps 1 and 2 in the discussion on current thickened flame models,

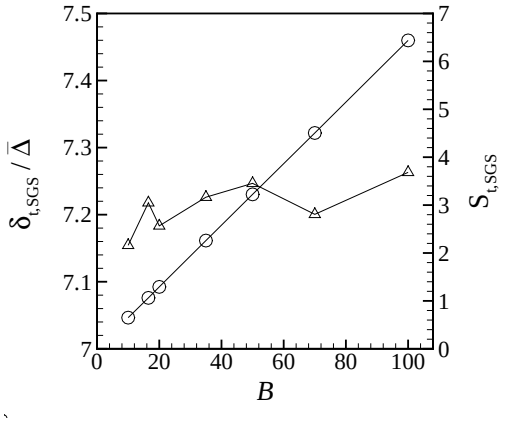

FIGURE 5. Behavior of $N_f = \delta_{t,SGS}/\bar{\Delta}$ ($\triangle$) and $S_{t,SGS}$ ($\bigcirc$) as a function of the preexponential B for a one-dimensional adaptive thickened flame with $N_z = 64$, $L_z = 0.75$, $Re = 20000$, $Pr = 0.7$, $Le = 1.0$, $C_f = 2.54$, $\alpha_1 = 2.0$, $\alpha_2 = 0.9$, $\alpha = 0.4$, $\beta = 7.0$.

to increase the subgrid scale burning velocity to account for subgrid scale wrinkling.

Shown in Fig. 6 is the behavior of N_f and $S_{t,SGS}$ as a function of the model constant C_f, indicating the increased resolution of the flame with increasing C_f and the increased burning velocity of the flame due to the increased effective diffusivity.

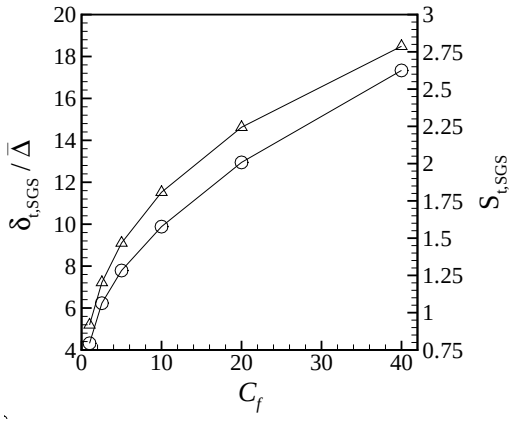

FIGURE 6. Behavior of $N_f = \delta_{t,SGS}/\bar{\Delta}$ ($\triangle$) and $S_{t,SGS}$ ($\bigcirc$) as a function of the model constant C_f for a one-dimensional adaptive thickened flame with $N_z = 64$, $L_z = 0.75$, $Re = 20000$, $Pr = 0.7$, $Le = 1.0$, $\alpha_1 = 2.0$, $\alpha_2 = 0.9$, $\alpha = 0.4$, $\beta = 7.0$, $B = 16.5$.

Shown in Fig. 7 is the behavior of N_f and $S_{t,SGS}$ during the propagation of a one-dimensional adaptive thickened flame through a structured nonuniform mesh. These results show that the adaptive thickened flame approach preserves Properties

1 and 2 over a large range of grid spacings, $\bar{\Delta}$, and Reynolds numbers for a one-dimensional flame and supports investigating its use in the current study of an LES of premixed turbulent combustion in stagnating turbulence.

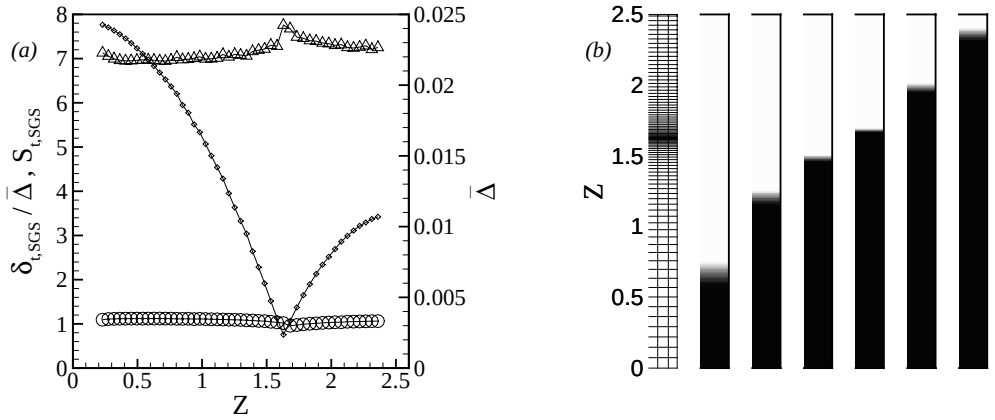

FIGURE 7. (*a*) Behavior of $N_f = \delta_{t,SGS}/\bar{\Delta}$ ($\triangle$) and $S_{t,SGS}$ ($\bigcirc$) during the propagation of a one-dimensional adaptive thickened flame through a structured nonuniform mesh, shown in (*b*) with contour plots of temperature at various times, with grid spacing $\bar{\Delta}$ ($\diamond$) and $N_z = 256$, $L_z = 2.5$, $Re = 20000$, $Pr = 0.7$, $Le = 1.0$, $C_f = 2.54$, $\alpha_1 = 2.0$, $\alpha_2 = 0.9$, $\alpha = 0.4$, $\beta = 7.0$, $B = 16.5$.

Applying this adaptive flame thickening technique to the filtered energy and species equations, Eqs. (11) and (12) respectively, using the eddy diffusivity models in Eqs. (16) and (17), leads to

$$\frac{\partial \bar{\rho}\tilde{T}}{\partial t} + \frac{\partial \bar{\rho}\tilde{u}_j\tilde{T}}{\partial x_j} = \frac{\partial}{\partial x_j}\left\{\left(\frac{\tilde{\mu}}{RePr} + \frac{C\bar{\Delta}^2\bar{\rho}|\tilde{S}_{ij}|}{Pr_t} + C_f\bar{\Delta}_f^{\alpha_1}\bar{\rho}B\left|\frac{\partial\tilde{T}}{\partial x_j}\right|\right)\frac{\partial\tilde{T}}{\partial x_j}\right\} + \frac{1}{\bar{\Delta}_f^{\alpha_2}}\tilde{w}_P \ , \tag{21}$$

$$\frac{\partial \bar{\rho}\tilde{Y}_R}{\partial t} + \frac{\partial \bar{\rho}\tilde{u}_j\tilde{Y}_R}{\partial x_j} = \frac{\partial}{\partial x_j}\left\{\left(\frac{\tilde{\mu}}{RePrLe} + \frac{C\bar{\Delta}^2\bar{\rho}|\tilde{S}_{ij}|}{Sc_t} + C_f\bar{\Delta}_f^{\alpha_1}\bar{\rho}B\left|\frac{\partial\tilde{T}}{\partial x_j}\right|\right)\frac{\partial\tilde{Y}_R}{\partial x_j}\right\} - \frac{1}{\bar{\Delta}_f{}^{\alpha_2}}\tilde{w}_P \ , \tag{22}$$

where

$$\tilde{w}_P = B\bar{\rho}\tilde{Y}_R exp\left(\frac{-\beta(1-\tilde{T})}{1-\alpha(1-\tilde{T})}\right) \ , \tag{23}$$

and $\bar{\Delta}_f$ denotes a local filter length formed by an average of the local grid spacing in each direction.

2.4 Preliminary LES of stagnating turbulence

The main objective of this study is the development of an LES of premixed turbulent combustion in stagnating turbulence. During the development of LES for incompressible nonreactive turbulent flow, DNS were valuable for validating the LES simulations and models. However, the resolution requirements of a DNS of premixed turbulent combustion in a realistic configuration are beyond current computing capabilities. Validation of LES of PTC, therefore, will rely on the availability of experimental data. Although numerous experimental studies of PTC in stagnating turbulence have been reported in the literature (Cho and Law, 1986; Cho and Law, 1988; Cheng and Shepherd and Gokalp, 1989; Cheng and Shepherd, 1991; Yahagi *et al.*, 1992; Shepherd and Ashurst, 1992; Li *et al.*, 1994; Shepherd, 1996; Hirasawa *et al.*, 1998; Stevens *et al.*, 1998) only a few report comparisons between the turbulent hydrodynamic statistics in the cold flow and the reactive hot flow. In order to assess a modeled set of zero Mach number LES combustion equations, it is advantageous to have this experimental comparison. An accurate LES cold flow simulation can then be performed and deviations from experimental data in the reactive hot flow LES thus reflect the modeling difficulties associated with the inclusion of a heat releasing premixed flame.

Shown in Fig. 1 is the computational domain with an inert co-flow surrounding the isotropic turbulent reactive core flow. The nonreactive incompressible LES equations given by Eqs. (9), (10), and (15) are solved with the dynamic procedure (Akselvoll and Moin, 1995; Germano *et al.*, 1991; Germano, 1992). The size of the computational domain, $L_r \times L_\theta \times L_z$, the number of grid points in each direction, $N_r \times N_\theta \times N_z$, and the remaining simulation parameters are given in Table I, where Re_{S_L} is the Reynolds number based on the laminar burning velocity and Re_{jet} is the Reynolds number based on the mean axial velocity of reactive core jet. The physical parameters used in the simulation correspond to the experimental study reported by Cho and Law (1986) of a premixed turbulent flame stabilized in a stagnation flow.

To simulate isotropic turbulence exiting the reactive core flow jet nozzle an isotropic turbulent field was generated from a decaying isotropic turbulence calculation and interpolated onto a three-dimensional cylindrical mesh representing the reactive core flow jet nozzle. A plane is then passed through the cylindrical mesh, with a velocity equal to the mean axial flow velocity exiting the jet, onto which the isotropic velocity field is interpolated at each time step. The velocity on the plane is used as the inlet velocity field for the reactive core jet.

$L_r \times L_\theta \times L_z$	$N_r \times N_\theta \times N_z$	Re_{S_L}	Re_{jet}	Fr
$2.0 \times 2.0\pi \times 1.5$	$96 \times 64 \times 64$	1400	13650	0.0

Table I. Simulation parameters for preliminary cold flow LES of stagnating turbulence.

Figure 8 is a contour plot of the axial velocity showing isotropic turbulence exiting the reactive core jet nozzle surrounded by a co-flow protecting the isotropic turbulent core.

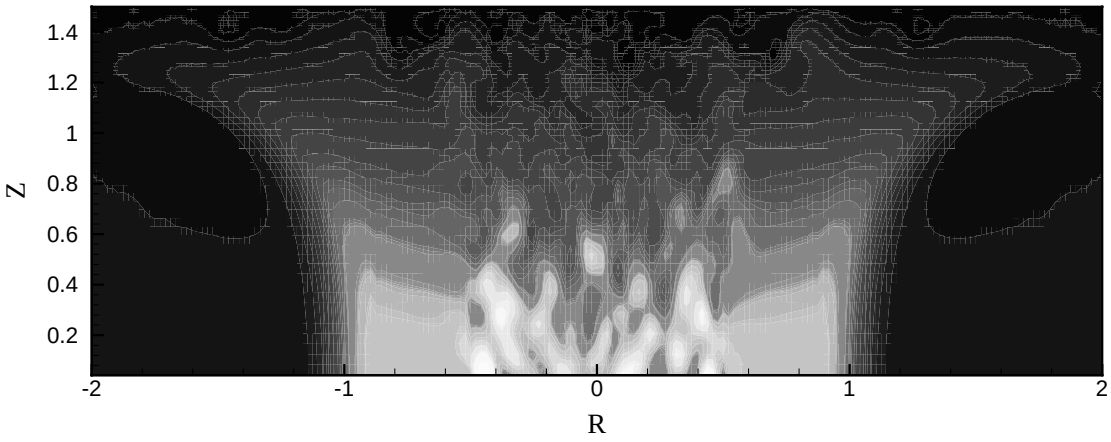

FIGURE 8. Contour plot of the instantaneous axial velocity showing the isotropic turbulent reactive core flow surrounded by a protective co-flow.

Shown in Fig. 9(a) is a comparison between simulation results and experimental data (Cho and Law, 1986) of the mean axial velocity along the centerline. Shown in Fig. 9(b) is a comparison between simulation results and experimental data (Cho and Law, 1986) of the mean axial velocity along two radial traverses.

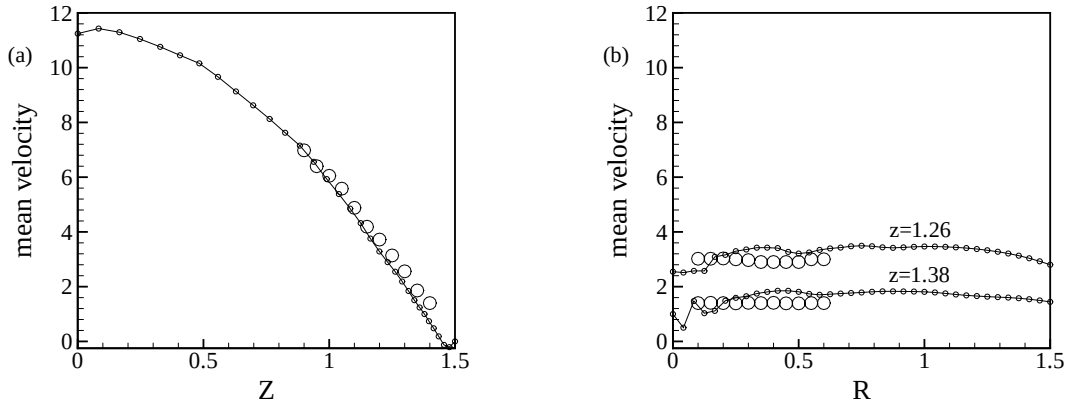

FIGURE 9. Comparisons between simulation results and experimental data (Cho and Law, 1986) of the mean axial velocity along (a) the centerline and (b) two radial traverses for the cold flow (nonreacting) case. ◯: experimental $\tilde{w}$. —○—: $\tilde{w}$.

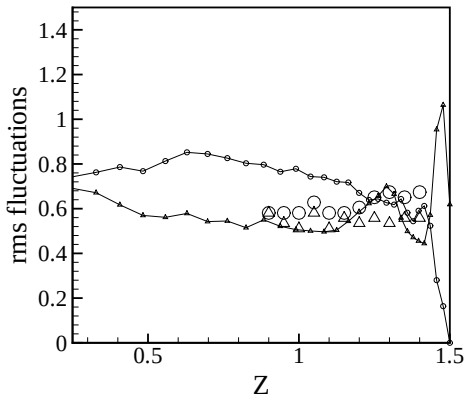

FIGURE 10. Comparison between simulation results and experimental data (Cho and Law, 1986) of the rms velocity fluctuations along the centerline in the cold flow (nonreacting) case. △: experimental u'. ◯: experimental w'. —△ —: u'; —○ —: w'.

Shown in Fig. 10 is a comparison between the radial and axial rms velocity fluctuations from simulation results and experiment data (Cho and Law, 1986). A slight decay in the rms axial velocity fluctuations is observed.

2.5 Preliminary LES of PTC in stagnating turbulence

In this section are presented preliminary results from an LES of PTC in stagnating turbulence using the modeled set of zero Mach number LES combustion equations presented above with the adaptive thickened flame approach.

In this preliminary reactive LES, the classical Smagorinsky model is used for the subgrid scale stresses in an effort to save computational time and cost. The expression

$$\bar{\Delta}_f = \frac{1}{2}(\Delta_r + \Delta_z)$$

is used in the temperature and species equations, Eqs. (21) and (22) respectively. The simulation parameters, in addition to those given in Table I, are given in Table II. At the lower and upper boundaries Dirichlet conditions are applied to the temperature and species equations with $T = 1$ and $Y_R = 0$ at the upper boundary, $T = 0$ at the lower boundary, $Y_R = 0$ outside the reactive core jet on the lower boundary, and $Y_R = 1$ inside the reactive core jet on the lower boundary. Neumann boundary conditions are applied to all variables at the outer sides of the domain.

Pr	Le	α	β	B	C_f
0.7	1.0	0.8	7.0	70.0	5.0

Table II. Simulation parameters, together with parameters given in Table I, for preliminary reactive hot flow LES of PTC in stagnating turbulence.

In Fig. 11 is a contour plot of the instantaneous axial velocity showing the rapid acceleration of the gas through the thickened flame. Shown in Fig. 12 are contour plots of the instantaneous temperature, species mass fraction, and reaction rate.

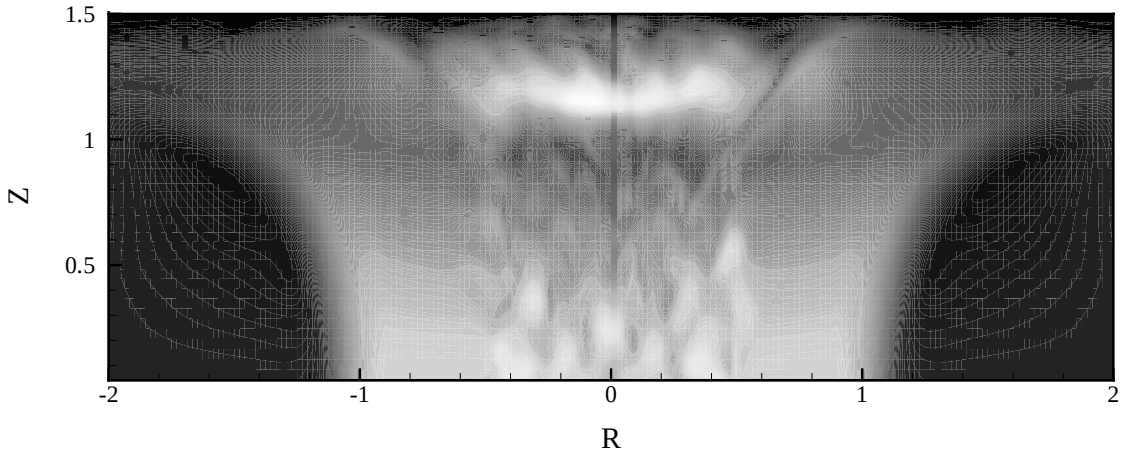

FIGURE 11. Contour plot of the instantaneous axial velocity showing the acceleration of the isotropic turbulent reactive core flow through the thickened flame.

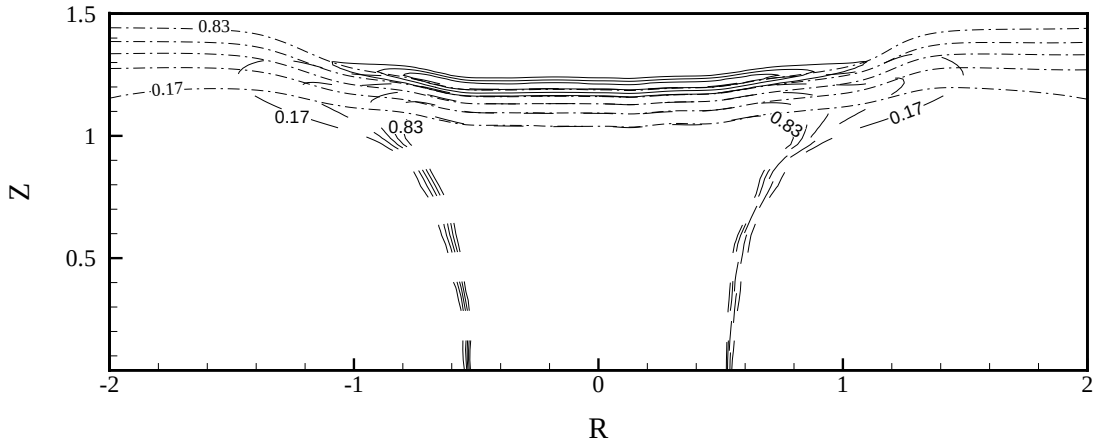

FIGURE 12. Contour plots of the instantaneous temperature ($- \cdot -$), species mass fraction ($-\ -$), and reaction rate (———).

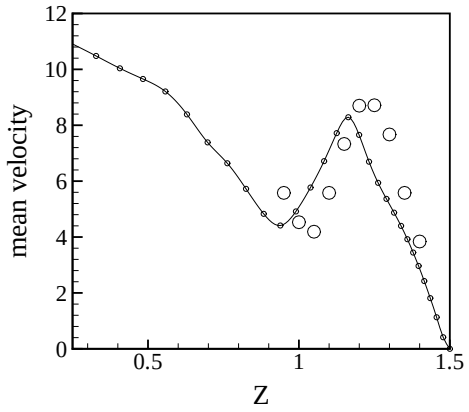

FIGURE 13. Comparison between simulation results and experimental data (Cho and Law, 1986) of the mean axial velocity along the centerline in the hot flow (reacting) case. ◯: experimental $\tilde{w}$. —○ —: $\tilde{w}$.

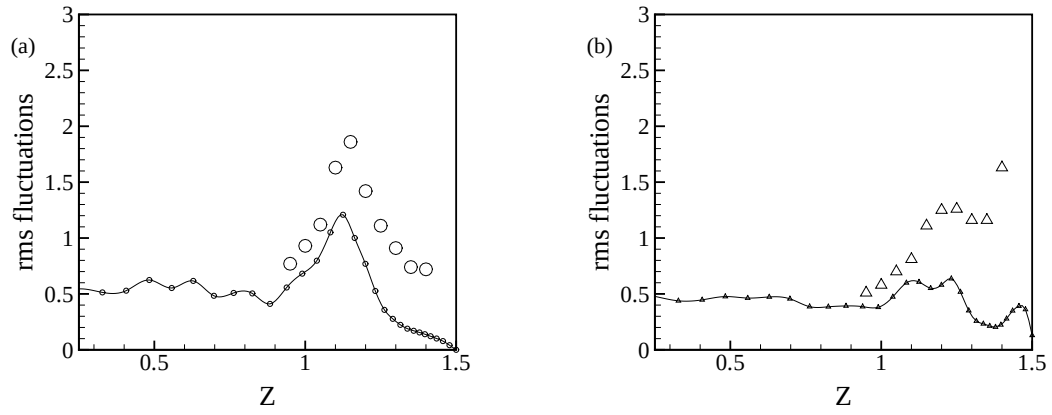

FIGURE 14. Comparison between simulation results and experimental data (Cho and Law, 1986) of the (a) axial and (b) radial rms velocity fluctuations along the centerline in the hot flow (reacting) case. △: experimental u'. ◯: experimental w'. —△ —: u'; —○ —: w'.

With the low turbulence intensity ($u'/S_L < 1$) and small hydrodynamic length scales produced by the turbulence generating grid in the reactive core jet nozzle, the thickened flame appears reasonably smooth. This is perhaps a drawback of this configuration for investigating LES of PTC. However, one of the key aspects in developing LES of PTC lies in reaction rate modeling and subsequent proper prediction of the subgrid scale turbulent burning velocity. Although large scale topology features are not present in the stagnating turbulence configuration, this configuration is well suited to testing subgrid scale reaction rate models as the subgrid scale turbulent burning velocity can be conveniently extracted from the simulations and numerous experimental studies provide data on the turbulent burning velocity of

premixed flames in stagnating turbulence.

Shown in Fig. 13 is a comparison of the mean axial velocity along the centerline between simulation results and experimental data. Shown in Fig. 14 is a comparison between simulation predictions and experimental data of the axial and radial rms velocity fluctuations along the centerline. Due to the preliminary nature of this simulation and the computational time and cost, the statistics were collected from only a small number of dumped fields over a short interval resulting in the observed fluctuations of the mean quantities.

3. Future plans

The simulations presented represent a preliminary investigation to test the developed code, the technique used to create an isotropic turbulent velocity field at the reactive core jet nozzle exit, and the adaptive thickened flame approach. It has been found that, although the adaptive thickened flame approach has potential, the major drawbacks are (a) its physically artifical nature and (b) the large effective diffusivity that is required to sufficiently thicken the flame results in excess computational time using the current fully explicit scheme due to the very small times steps required by the small value of Δ_θ at the centerline. Due to the presence of the magnitude of the temperature gradient in the diffusivity term, implicit treatment in the θ direction of the diffusive terms is not straightforward. Future work will focus on: (a) construction and validation of an isotropic turbulent field with the correct spectral properties to use at the reactive core jet nozzle exit, (b) examination of different models for the reaction rate expression which will hopefully alleviate the severe computational cost while providing a more physically attractive approach over the artificial flame thickening technique, and (c) further consideration regarding the boundary layer at the plate and the application of LES wall models.

Acknowledgments

The author would like to acknowledge and express his gratitude to Dr. B. J. Boersma for his invaluable and unconditional assistance and guidance during the development of the LES code used in this study. The author would also like to acknowledge Professor K. N. C. Bray and Professor T. Poinsot for their helpful comments and suggestions.

REFERENCES

Akselvoll, K. & Moin, P. 1995 Large eddy simulation of turbulent confined coannular jets and turbulent flow over a backward facing step. *Ph.D. Thesis*, Department of Mechanical Engineering, Stanford University.

Angelberger, C., Veynante, D., Egolfopoulos, F. & Poinsot, T. 1998 Large eddy simulations of combustion instabilities in premixed flames. *Proceedings of the Summer Program*, Center for Turbulence Research, NASA/Stanford Univ., 61-82.

Boger, M., Veynante, D., Boughanem, H. & Trouvé, A. 1998 Direct numerical simulation analysis of flame surface density concept for large eddy simulation of turbulent premixed combustion. *Twenty-Seventh Symp. (Intl) on Combustion*, The Combustion Institute, 917-925.

Boughanem, H. & Trouvé, A. 1998 The domain of influence of flame instabilities in turbulent premixed combustion. *Twenty-Seventh Symp. (Intl) on Combustion*, The Combustion Institute, 971-978.

Bray, K. N. C., Champion, M., Libby, P. A. 1991 Premixed flames in stagnating turbulence: Part 1. The general formulation for counterflowing streams and gradient models for turbulent transport. *Combust. Flame.* **84,** 391-410.

Bray, K. N. C., Champion, M., Libby, P. A. 1994 Flames in stagnating turbulence. *Turbulent Reacting Flows*, Libby, P.A. & Williams, F.A. editors, Academic Press.

Bray, K. N. C., Champion, M., Libby, P. A. 1998 Premixed flames in stagnating turbulence: Part II. The mean velocities and pressure and the Damköhler number. *Combust. Flame.* **112,** 635-654.

Bray, K. N. C., Champion, M. & Libby, P. A. 1999 Premixed flames in stagnating turbulence: Part IV. A new theory for the Reynolds stresses and Reynolds fluxes assessed and exploited in impinging flows. *Submitted to Combust. Flame.*

Butler, T. D. & O'Rourke, P. J. 1977 A numerical method for two-dimensional unsteady reacting flows. *Sixteenth Symp. (Intl) on Combustion*, The Combustion Institute, 1503-1515.

Chen, J. H. & Im, H. G. 1998 Correlation of flame speed with stretch in turbulent premixed methane-air flames. *Twenty-Seventh Symp. (Intl) on Combustion*, The Combustion Institute, 819-826.

Chen, J. H. & Echekki, T. & Kollmann, W. 1999 The mechanism of two-dimensional pocket formation in lean premixed methane-air flames with implications to turbulent combustion. *Combust. Flame.* **116,** 15-48.

Cheng, R. K. & Shepherd, I.G. & Gokalp, I. 1989 A comparison of the velocity and scalar spectra in premixed turbulent flames. *Combust. Flame.* **78,** 205-221.

Cheng, R. K. & Shepherd, I. G. 1991 The influence of burner geometry on premixed turbulent flame propagation. *Combust. Flame.* **85,** 7-26.

Cho, P. & Law, C. K., Hertzberg, J. R. & Cheng, R. K. 1986 Structure and propagation of turbulent premixed flames stabilized in a stagnation flow. *Twenty-First Symp. (Intl) on Combustion*, The Combustion Institute, 1493-1499.

Cho, P. & Law, C. K., Cheng, R. K. & Shepherd, I. G. 1988 Velocity and scalar fields of turbulent premixed flames in stagnation flow. *Twenty-Second Symp. (Intl) on Combustion*, The Combustion Institute, 739-745.

Colin, O. & Ducros, F., Veynante, D., Poinsot, T. 1999 A thickened flame model for large eddy simulations of turbulent premixed combustion. *private communication.*

Echekki, T. & Chen, J. H. 1996 Unsteady strain rate and curvature effects in turbulent premixed methane-air flames. *Combust. Flame.* **106,** 184-202.

Erlebacher, G., Hussaini, M. Y., Speziale, C. G., Zang, T. A. 1990 *ICASE Report 90-76*, ICASE/NASA Langley Research Center.

Germano, M., Piomelli, U., Moin, P., Cabot, W. H. 1991 A dynamic subgrid-scale eddy viscosity model. *Phys. Fluids A.* **3**(7)**,** 1760-1765.

Germano, M. 1992 Turbulence: the filtering approach. *J. Fluid Mech.* **238,** 325-336.

Givi, P. 1994 Spectral and random vortex methods in turbulent reacting flows. *Turbulent Reacting Flows*, Libby, P.A. & Williams, F.A. editors, Academic Press.

Haworth, D. C. & Poinsot, T. J. 1992 Numerical simulations of Lewis number effects in turbulent premixed flames. *J. Fluid Mech.* **244,** 405-436.

Helie, J. & Trouvé, A. 1998 Turbulent flame propagation in partially premixed combustion. *Twenty-Seventh Symp. (Intl) on Combustion*, The Combustion Institute, 891-898.

Hirasawa, T., Ueda, T., Matsuo, A. & Mizomoto, M. 1998 Effect of oscillatory stretch on the flame speed of wall-stagnating premixed flame. *Twenty-Seventh Symp. (Intl) on Combustion*, The Combustion Institute, 875-882.

Im, H. G. & Lund, T. S., Ferziger, J. H. 1996 Large eddy simulation of turbulent front propagation with dynamic subgrid models. *Phys. Fluids.* **9,** (12), 3826-3833.

Kostiuk, L. W., Shepherd, I. G., Bray, K. N. C. 1999 Experimental study of premixed turbulent combustion in opposed streams: Part III. Spatial structure of flames. *Combust. Flame.* **118,** 129-139.

Li, S. C., Libby, P. A. & Williams, F. A. 1994 Experimental investigation of a premixed flame in an impinging turbulent stream. *Twenty-Fifth Symp. (Intl) on Combustion*, The Combustion Institute, 1207-1214.

Lindstedt, R. P. & Vaos, E. M. 1998 Second moment modeling of premixed turbulent flames stabilized in impinging jet geometries. *Twenty-Seventh Symp. (Intl) on Combustion*, The Combustion Institute, 957-962.

Lindstedt, R. P. & Vaos, E. M. 1999 Modeling of premixed turbulent flames with second moment methods. *Combust. Flame.* **116,** 461-485.

Louch, D. S. 1998 Vorticity and turbulent transport in premixed turbulent combustion. *Ph.D. Thesis*, Trinity Hall, University of Cambridge, England.

Louch, D. S., Bray, K. N. C. 1999 Vorticity in unsteady premixed flames: Vortex pair-premixed flame interactions under imposed body forces and various

degrees of heat release and laminar flame thickness. *accepted for publication in Combust. Flame.*

Louch, D. S. & Bray, K. N. C. 1998 Vorticity and scalar transport in premixed turbulent combustion. *Twenty-Seventh Symp. (Intl) on Combustion*, The Combustion Institute, 801-810.

Peters, N. 1992 A spectral closure for premixed turbulent combustion in the flamelet regime. *J. Fluid Mech..* **242,** 611-629.

Poinsot, T., Candel, S. & Trouvé, A. 1996 Applications of direct numerical simulation to premixed turbulent combustion. *Prog. Energy Combust. Sci..* **21,** 531-576.

Pope, S. B. 1988 The evolution of surfaces in turbulence. *Int. J. Engng. Sci..* **26,** (5), 445-469.

Prasad, R. O. S. & Gore, J. P. 1999 An evaluation of flame surface density models for turbulent premixed jet flames. *Combust. Flame.* **116,** 1-14.

Rhee, C. W., Talbot, L. & Sethian, J. A. 1995 Dynamical behaviour of a premixed turbulent open V-flame. *J. Fluid Mech.* **300,** 87-115.

Rutland, C. J. & Cant, R. S. 1994 Turbulent transport in premixed flames. *Proceedings of the Summer Program*, Center for Turbulence Research, NASA/ Stanford Univ., 75-94.

Shepherd, I. G. & Ashurst, W. T. 1992 Flame front geometry in premixed turbulent flames. *Twenty-Fourth Symp. (Intl) on Combustion*, The Combustion Institute, 485-491.

Shepherd, I. G. 1996 Flame surface density and burning rate in premixed turbulent flames. *Twenty-Sixth Symp. (Intl) on Combustion*, The Combustion Institute, 373-379.

Smith, T. M. & Menon, S. 1996 The structure of premixed flames in a spatially evolving turbulent flow. *Combust. Sci. and Tech.* **119,** 77-106.

Stevens, E. J., Bray, K. N. C. & Lecordier, B. 1998 Velocity and scalar statistics for premixed turbulent stagnation flames using PIV. *Twenty-Seventh Symp. (Intl) on Combustion*, The Combustion Institute, 949-955.

Trouvé, A. & Poinsot, T. 1994 The evolution equation for the flame surface density in turbulent premixed combustion. *J. Fluid Mech.* **278,** 1-31.

Veynante, D., Trouvé, A., Bray, K. N. C. & Mantel, T. 1997 Gradient and counter-gradient scalar transport in turbulent premixed flames. *J. Fluid Mech.* **332,** 263-293.

Veynante, D. & Poinsot, T. 1997 Large eddy simulation of combustion instabilities in turbulent premixed burners. *Annual Research Briefs*, Center for Turbulence Research, NASA/Stanford Univ., 253-274.

Veynante, D. & Poinsot, T. 1997b Effects of pressure gradients on turbulent premixed flames. *J. Fluid Mech.* **353,** 83-114.

Veynante, D., Trouvé, A., Bray, K. N. C. & Mantel, T. 1997 Gradient and counter-gradient scalar transport in turbulent premixed flames. *J. Fluid Mech.* **332,** 263-293.

Yahagi, Y., Ueda, T. & Mizomoto, M. 1992 Extinction mechanism of lean methane-air turbulent premixed flame in a stagnation point flow. *Twenty-Fourth Symp. (Intl) on Combustion*, The Combustion Institute, 537-542.

Zhang, S. & Rutland, C. J. 1995 Premixed flame effects on turbulence and pressure-related terms. *Combust. Flame.* **102,** 447-461.